INORGANIC CHEMISTRY FRONTIERS

RESEARCH ARTICLE

View Article Online
View Journal

Cite this: DOI: 10.1039/d6qi00236f

Copper(II) outcompetes other metal ions in spike fragment complexation, driving ROS-dependent oxidation

Monika Katarzyna Lesiów, *[a] Lajos Nagy,[b] Antal Galvácsi[c] and Csilla Kállay [c]

The SARS-CoV-2 spike protein plays a central role in viral entry into lung cells and has been implicated in promoting reactive oxygen species (ROS) formation in COVID-19 patients. Despite extensive research, the molecular factors contributing to spike-associated redox activity remain insufficiently understood, particularly the influence of metal ions. Here, we investigate the coordination properties of biologically essential metal ions (Cu^{2+}, Fe^{2+}, Fe^{3+}, Mn^{2+}, Co^{2+}, Zn^{2+}) and the potentially essential (Ni^{2+}) with modified spike protein fragments (Ac-ADGKAHFPRE-NH_2, **S4**, and Ac-HDGKAAFPRE-NH_2, **S5**). Our studies showed that Cu^{2+} ions form the most stable complexes at pH 6.7 (lung conditions). Potentiometric and spectroscopic analysis revealed distinct coordination modes, with a predominant 3N{N_{im}, $2N^-$} for **S4** and 1N {N_{im}} for **S5**. Electrochemical and EPR studies demonstrated that Cu^{2+}-peptide complexes undergo redox cycling, including their reduction to Cu^+. This redox activity drives ROS production, confirmed by ascorbate consumption, rhodamine 6G degradation and gel electrophoresis, which identified $^{\bullet}OH$, $^1O_2$ and $O_2^{\bullet-}$. The generated ROS induce DNA double-strand breaks, with the Cu(II)-Ac-ADGKAHFPRE-NH_2 complex (**CuS4**) exhibiting higher oxidative potential than Cu(II)-Ac-HDGKAAFPRE-NH_2 (**CuS5**). Peptide oxidation in Cu(II)/H_2O_2 systems further showed that ROS produced by these complexes directly oxidize specific amino acid residues. In the presence of ascorbic acid, oxidation occurs mainly at the histidyl residue, whereas in its absence, selective lysyl oxidation yields α-aminoadipic acid, demonstrating redox-dependent, residue-specific oxidative pathways.

Received 1st February 2026,
Accepted 17th April 2026

DOI: 10.1039/d6qi00236f

rsc.li/frontiers-inorganic

Introduction

Oxidative stress, driven by excessive production of reactive oxygen species (ROS), is strongly associated with lung injury and respiratory dysfunction.[1] Elevated ROS levels have been reported among patients with asthma.[2] ROS are also associated with chronic obstructive pulmonary disease (COPD)[3] and the development of adult respiratory distress syndrome (ARDS).[4–6] Moreover, oxidative stress promotes proliferation and angiogenesis, playing a significant role in lung cancer initiation and development.[7] In severe COVID-19 patients, neutrophils display significantly increased ROS production, with a nine-fold higher median value compared to healthy individuals.[8]

One of the proposed mechanisms involves the participation of SARS-CoV-2 spike protein, a key factor responsible for viral entry into host cells, in ROS generation.[9,10] Youn and colleagues demonstrated high levels of superoxide anion radicals in primary bovine aortic endothelial cells after treatment with the spike protein.[11] Greenberger *et al.* confirmed that the spike protein initiates ROS formation, induces double-strand DNA breaks, activates transforming growth factor-beta pathways and promotes senescence in human lung epithelial cancer cells (H460 and IB3), as well as in K18-hACE2 mouse lungs.[12] Barhoumi and collaborators further showed that the spike protein triggers oxidative stress, intracellular calcium ions release, inflammation, and apoptosis in THP-1-like macrophage.[13] Notably, all of these studies were conducted in the absence of metal ions.

We hypothesize that ROS production induced by the spike protein can be further enhanced by transition metal ions. Metals essential for life, such as copper, iron, manganese, cobalt and zinc, must be tightly regulated in the human organism, whereas others, *e.g.* nickel or chromium, are considered possibly essential.[14] Literature reports suggest that transition metal ions may play an important role in the molecular mechanisms of COVID-19. Structural studies indicate that SARS-CoV-2 proteins frequently coordinate zinc ions, while others reports describe alterations in metal homeostasis in COVID-19 patients.[15] Elevated iron ion levels are widely docu-

[a]*Faculty of Chemistry, University of Wrocław, F. Joliot-Curie 14, 50-383 Wrocław, Poland. E-mail: monika.lesiow2@uwr.edu.pl*
[b]*Department of Applied Chemistry, University of Debrecen, H-4032 Debrecen, Hungary*
[c]*Department of Inorganic and Analytical Chemistry, University of Debrecen, H-4032 Debrecen, Hungary*

mented and considered contributors to disease pathogenesis,[16,17] whereas increased serum concentrations of nickel, manganese, and cobalt ions suggest possible interactions with viral proteins.[18–20] Notably, copper ion levels increase following SARS-CoV-2 entry into lung cells and subsequent inflammation, further highlighting the relevance of transition metal ions in COVID-19 pathology.[21,22] Moreover, complexes of the above-mentioned metal ions (except zinc) can participate in Fenton reactions, generating highly reactive hydroxyl radicals.[23]

ROS can oxidize amino acid residues, cleave peptide bonds, and promote protein aggregation.[24] For example, lysyl residues may be oxidatively converted into α-aminoadipic acid, which is recognized as a biomarker of pathological conditions, including COVID-19.[25] ROS also cause modification of nitrogen bases and single- or double-strand DNA breaks.[24,26] Free radicals further attack polyunsaturated fatty acids, resulting in lipid peroxidation.[27] These processes may lead to pathogenic conditions, including cardiovascular and neurodegenerative diseases, cancer and diabetes.[28–33]

In this article, we investigate two peptide models designed by us based on the amino acid sequence of the SARS-CoV-2 spike protein (Fig. 1). Within the spike protein sequence, two histidyl residues (H^{1083} and H^{1088}) are located in close proximity. The H^{1083} residue is known to undergo mutation to glutamine.[34] Accordingly, two peptides were designed: Ac-ADGKAHFPRE-NH_2 (**S4**) and Ac-HDGKAAFPRE-NH_2 (**S5**), in which H^{1083} and H^{1088} are selectively replaced by alanine to explore the role of histidyl residues in metal binding (Fig. 1). These sequences position the histidyl residue differently within the peptide chain.

Our goals were to: (i) determine whether His(Ala) substitution preserves metal-binding ability; (ii) identify which histidyl residue initiates the coordination process; (iii) compare the ROS production potential of both complexes; (iv) assess the impact of the generated ROS on DNA; and (v) evaluate peptide oxidation, identify amino acid residues susceptible to ROS-induced modification, and determine the corresponding oxidation products.

Together, these objectives aim to identify which transition metal ions most effectively coordinate to spike-derived peptides and to clarify how such interactions may promote ROS-driven oxidative modifications that could influence the course and severity of COVID-19.

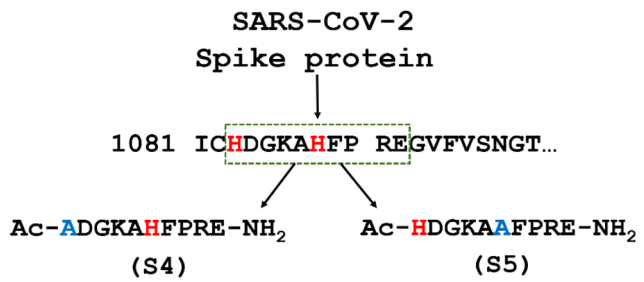

Fig. 1 Two peptide fragments selected for study and designed based on the SARS-CoV-2 spike protein sequence.

Results and discussion

Interaction of peptides with transition metal ions (essential/possible essential for life)

We decided to start our research by determining the ability of two Ac-**A**DGKA**H**FPRE-NH_2 (**S4**) and Ac-**H**DGKA**A**FPRE-NH_2 (**S5**) ligands to bind transition metal ions which are considered essential for life (copper, iron, manganese, cobalt and zinc) and possibly essential for life as nickel ions. The potentiometric data revealed that in the case of Zn(II), Co(II) and Fe(III) ions mainly hydroxo complexes are formed in the solution (Tables S1 and S2). Fe(II) ions coordinate to peptides forming weak complexes, while Mn(II) does not form complexes with the studied ligands at all. Cu(II) and Ni(II) ions turn out to have the highest potential to form complexes with **S4** and **S5** ligands (Tables S1–S4). However, the stability constants calculated for the complexes with these metal ions show that Cu(II) ions form more stable complexes than Ni(II) ones (Tables S2 and S4). For this reason, all subsequent experiments were performed exclusively with Cu(II) ions. Considering that Cu levels are elevated in the lung tissues of patients with pulmonary inflammatory conditions,[35,36] we propose that the **S4** and **S5** ligands may coordinate Cu(II) ions in the human body. The structure of the Cu(II) complexes with **S4** and **S5** ligands was determined by the spectroscopic methods (UV-Vis, CD and EPR) as well as MS (but in gas phase to support the formation of the appropriate species). Research in the solution was conducted in a wide pH range (2.5–10.5), however the most interesting for us was to know the structure of the complexes at lung pH (pH 6.7). Thus, in the main article we focus on the structure of the complexes formed at pH 6.7 and the characteristics of other species are included in the supplementary material.

The species distribution diagram revealed that around 80% of the solution at pH 6.7 consists of $CuH_{-1}L$ species for **S4** peptide, while around 50% of the CuHL and 20% of CuL complexes dominate in the solution for **S5** ligand (Fig. 2). The stoichiometry of $CuH_{-1}L$ species and the calculated $\log K^*$ (−14.73) confirmed that metal ions are bound by three nitrogen atoms $3N\{N_{im}, 2N^-\}$.[37] The calculated $\log K^*$ value is lower than that determined for the Cu(II) complex with another spike protein fragment, Ac-ELDKYFKNH-NH_2, studied by us previously (Table 1).[38] This indicates that the Cu(II)-Ac-ADGKAHFPRE-NH_2 (**CuS4**) complex is slightly less stable than Cu(II)-Ac-ELDKYFKNH-NH_2 in the lung environment. However, the **CuS4** complex has comparable stability to the Cu(II)-WSHPQFEK-NH_2 system, which is also a fragment of the spike protein of the SARS-CoV-2 virus (Table 1).[38]

The maximum of absorption band in the UV-Vis spectrum at 597 nm (λ_{max} = 584 nm from the Prenesti equation),[39] CT transitions in the CD spectrum $N_{im(\pi 2)} \rightarrow Cu(II)$ at 253 nm and CT at 336 nm being the mixture of two bands: $N^-_{(amide)} \rightarrow$ Cu

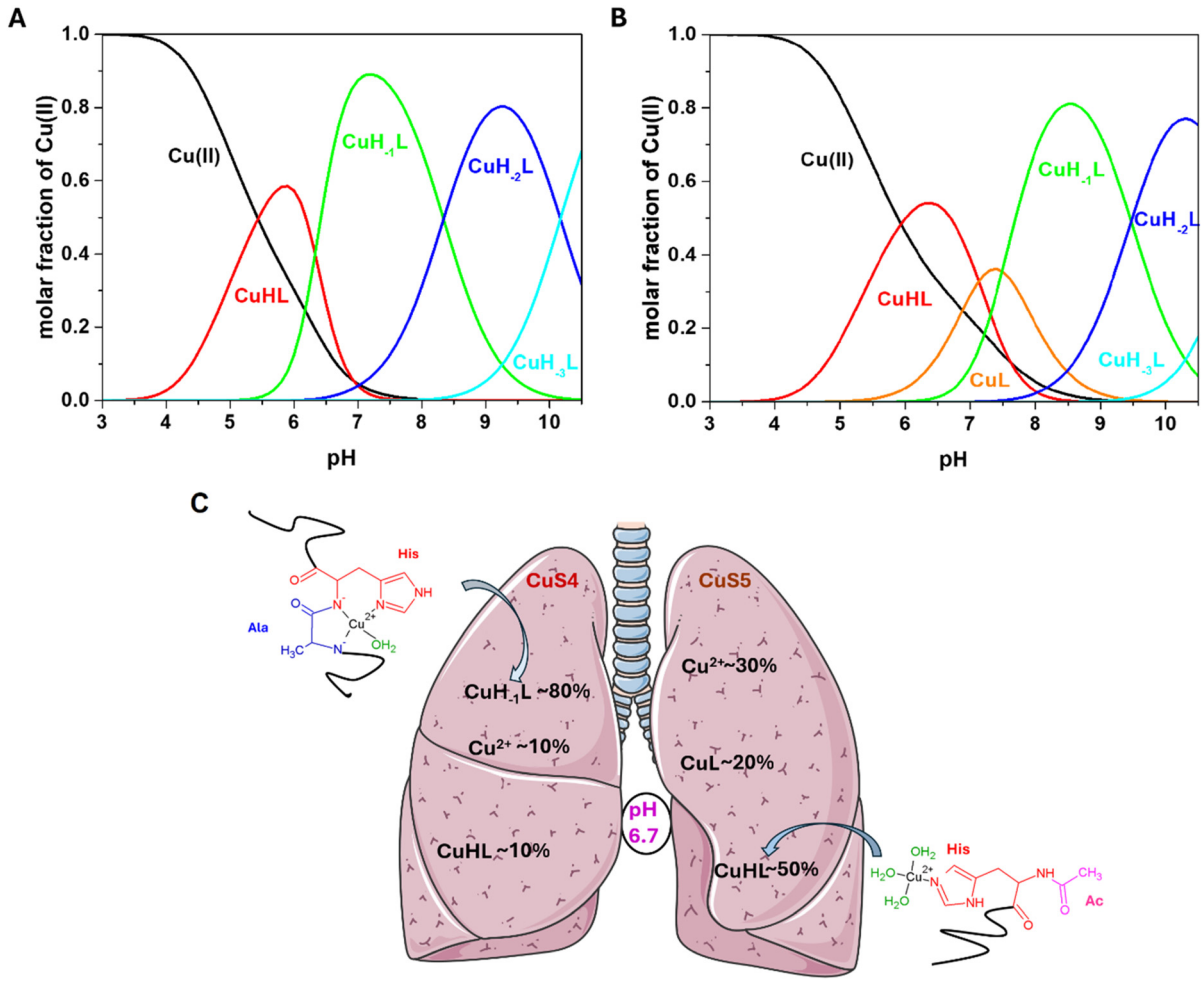

Fig. 2 Species distribution diagram of the (A) **CuS4** and (B) **CuS5** complexes as a function of pH (Cu : L = 1 : 1 molar ratio; [Cu(II)] = 0.001 M), while (C) proposed schematic structures of $CuH_{-1}L$ of **S4** ligand and CuHL of **S5** peptide dominant at lung pH (pH 6.7) along with the percentage of other species and Cu(II) ions present at this pH value.

Table 1 The calculated log *K** and pCu values for mononuclear Cu(II) complexes (Cu(II)-Ac-ADGKAHFPRE-NH_2, **CuS4** and Cu(II)-Ac-HDGKAAFPRE-NH_2, **CuS5**) and previously studied by us complexes with other spike protein fragments (Cu(II)-Ac-ELDKYFKNH-NH_2, **CuL1** and Cu(II)-Ac-WSHPQFEK-NH_2, **CuL2**)

	log *K** [a]				pCu[d]
Form	1N $\{N_{im}\}$ [b]	2N $\{N_{im}, N^-\}$	3N $\{N_{im}, 2N^-\}$	4N $\{N_{im}, 3\ N^-\}$	
CuS4	−2.07	—	−14.73	−23.07	3.88
CuS5	−2.51	−9.64	−17.13	−26.60	3.37
CuL1 [c]	−2.39	—	−14.00	−22.05	4.21
CuL2 [c]	−2.34	—	−15.16	−22.88	3.72

[a] The log *K** values are for the reaction: $Cu^{2+} + H_nL \rightleftarrows CuH_jL^{(2-n+j)+} + (n-j)H^+$; $\log K^* = \log\beta(CuH_jL) - \log\beta(H_nL)$ (where index *j* stands for the number of protons in the ligand coordinated to the metal ion and *n* denotes the number of protons of the coordinated ligand plus the protons released from the ligand during complexation). [b] 1N, 2N, 3N or 4N indicate the number of nitrogen atoms directly coordinated to Cu(II) ion, whereas N_{im} and N^- indicate nitrogen atoms of imidazole and amide groups, respectively. [c] Ref. 38. [d] pCu values were calculated at $C_{Cu(II)} = C_{peptide} = 2$ mM at pH 6.7.

(II) and $N_{im(\pi1)} \rightarrow$ Cu(II) as well as EPR parameters ($g_\parallel$ (g_{zz}) = 2.224, $g_\perp$ (g_{xx}) = 2.049, $g_\perp$ (g_{yy}) = 2.058, $^{Cu}A_\parallel$ = 17.3 mT) are in agreement with proposed coordination mode (Table S5, Fig. S1, S2 and Fig. 3A).[40–42] Most probably the coordination process goes in *N*-terminal direction where stable 6- and 5-membered rings are formed. Moreover, the ESI-MS spectrum of the **CuS4** complex recorded in positive ion mode at a 1 : 1 metal to ligand (M : L) molar ratio also confirms the formation of the $CuH_{-1}L$ complex but in the gas phase, as evidenced by the molecular ion observed at *m*/*z* 1229.6 Da corresponding to $CuH_{-1}L^+$ (Fig. 3B).

In turn, in the case of CuHL and CuL species for the **S5** ligand, the stoichiometry and calculated log *K** values (−2.51 for CuHL and −9.64 for CuL, respectively) suggest binding of Cu(II) ion by one imidazole from His residue for CuHL and existence of two nitrogen complex in the case of CuL species (Fig. 2B and Table 1).[38,43] The calculated log *K** value (−2.51) for the 1N$\{N_{im}\}$ coordination mode of the **CuS5** complex is comparable to the values obtained for the Cu(II) complexes with the Ac-ADGKAHFPRE-NH_2, Ac-ELDKYFKNH-NH_2 and

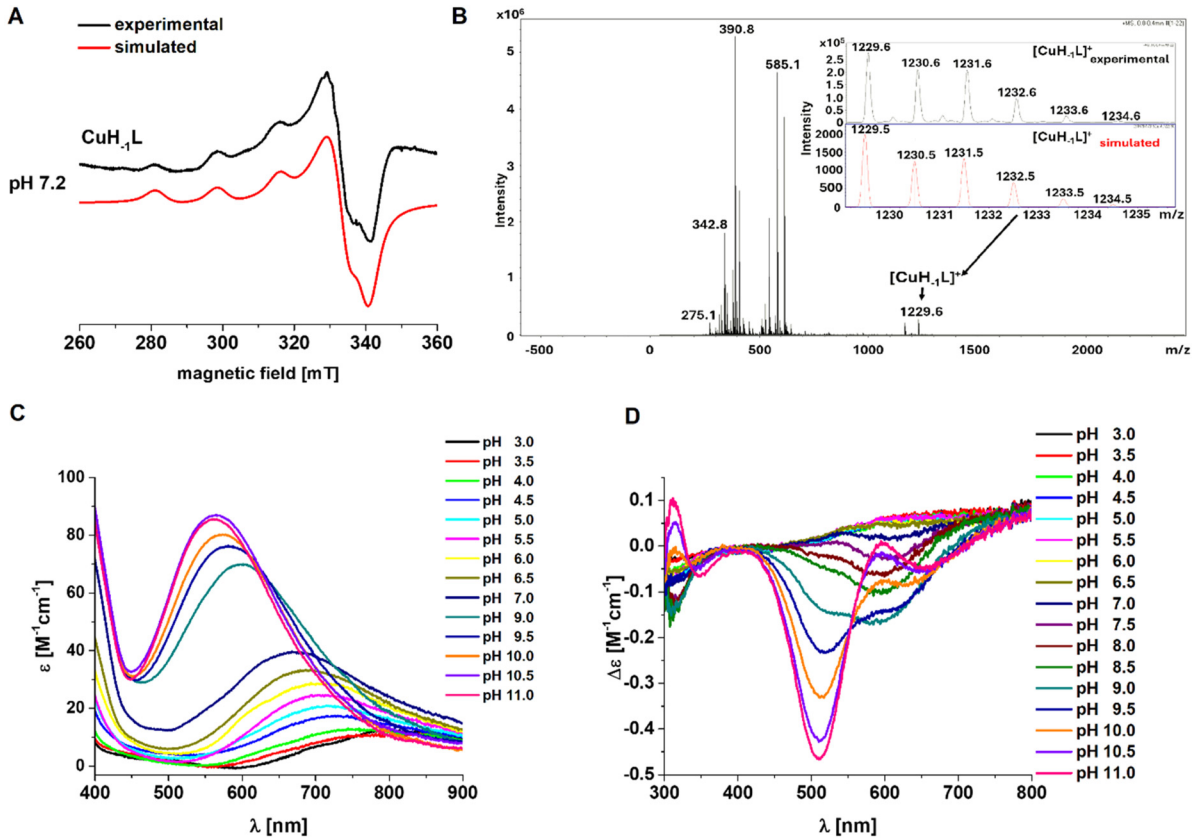

Fig. 3 Coordination studies conducted for the Cu(II)-Ac-ADGKAHFPRE-NH_2 (**CuS4**) and Cu(II)-Ac-HDGKAAFPRE-NH_2 (**CuS5**) complexes: (A) EPR spectrum recorded for frozen (77 K) solutions of **CuS4** complex at pH 7.2 (Cu : L = 1 : 1, [Cu(II)] = 0.001 M); (B) ESI mass spectrum of the **CuS4** (Cu : L = 1 : 1 molar ratio) in aqueous solution (pH ~ 7) along with experimental and simulated spectra of $[CuH_{-1}L]^+$ molecular ion (m/z = 1229.6 Da); (C) electronic absorption spectra of the **CuS5** complex as a function of pH (1 : 1 M : L molar ratio, [Cu(II)] = 0.001 M); (D) CD spectra of the **CuS5** complex in the Vis region as a function of pH (1 : 1 M : L molar ratio, [Cu(II)] = 0.001 M).

WSHPQFEK-NH_2 peptides (Table 1).[38] The band at 693 nm in UV-Vis spectrum of CuHL species (λ_{max} = 760 nm predicted by Prenesti[39]) proves that one nitrogen donor atom binds to metal ion (Table S5 and Fig. 3C). The markedly shorter wavelength of the observed d–d transition compared to the predicted value suggests the presence of donor atoms other than water-derived oxygen atoms in the coordination sphere. These donors likely originate from the carboxylate groups of the Asp and Glu residues of the peptide.[44] No CT transitions and d–d bands were observed in CD spectrum (Fig. 3D and Fig. S3) and EPR parameters could not be obtained because of significant broadening of the lines. In turn, the calculated $pK_{a(1/0)}$ (7.49) value for CuHL ⇄ CuL + H^+ reaction confirms the involvement of first amide nitrogen in coordination process (Table S4).[45] However, the spectroscopic characteristics of CuL species cannot be done due to overlapping of uncomplexed Cu(II) ions and other species (CuHL and $CuH_{-1}L$) with this complex (Fig. 2B).

Redox properties

Cyclic voltammetry. The redox activity of Cu(II) complexes with **S4** and **S5** ligands was studied by cyclic voltammetry (CV). However, before starting these studies, the electrochemical measurement system was calibrated using $K_3[Fe(CN)_6]$ redox system (Fig. S4). No anodic or cathodic signals were observed in the voltammograms of the **S4** and **S5** ligands (Fig. S5A1 and B1). The signal observed at 0.032 V for the **CuS5** complex may be related to metal-centered oxidation within the complex (Fig. S5B2).[46] Anodic signals observed for both complexes at 0.707 V for **CuS4** and 0.678 V for **CuS5** are attributed to the oxidation of the histidyl residue within the Cu-peptide complex (Fig. S5A2 and B2).[46,47] Moreover, the presence of two cathodic peaks at 0.526 and 0.740 V for **CuS4** and at 0.484 and 0.693 V for **CuS5** indicates that the oxidized species undergoes a subsequent chemical or structural reorganization, leading to two distinct reducible forms (Fig. S5A2 and B2). This occurrence of two cathodic peaks, interpreted as arising from two distinct forms, has also been reported for other copper–peptide systems.[48] Overall, these results are consistent with a quasi-reversible, surface-confined redox process following an EC-type mechanism.

Reduction of Cu(II) ions in CuS4 and CuS5 complexes by ascorbic acid. The application of EPR spectroscopy enabled us to address whether the reduction of Cu(II) ions to Cu(I) occurs under the influence of ascorbic acid, and to determine which of the studied complexes (**CuS4** or **CuS5**) undergoes this reduction more rapidly. Cu(II) ions possess an unpaired elec-

tron, making them EPR-active. Upon reduction to Cu(I), the ions become diamagnetic, resulting in the disappearance of the EPR signal.

EPR spectra of both **CuS4** and **CuS5** complexes were recorded at pH 6.7, then immediately after the addition of ascorbic acid and again after one-hour of measurements. From the relative intensities of the spectra, the approximate percentage of Cu(II) ions reduction in each complex was estimated. The results are summarized in Table 2.

By comparing the percentages of reduced Cu(II) ions in both complexes immediately after the addition of ascorbic acid (approximately 50% for **CuS4** and 85% for **CuS5**), it can be concluded that the reduction of Cu(II) ions in the **CuS5** complex is both more extensive and significantly faster than in **CuS4**. After one hour of measurements, nearly complete reduction of metal ions is observed in the **CuS5** complex, whereas in **CuS4** the reduction of Cu(II) to Cu(I) increases to approximately 70%. This may indicate a greater potential of the **CuS5** complex to undergo redox reactions in the presence of ascorbic acid and generate reactive oxygen species (ROS). Therefore, in next step we decided to investigate the ability of both Cu(II) complexes to produce ROS.

Monitoring ROS generation

Ascorbic acid consumption assay. Knowing that Cu(II) ions can undergo reduction within the complexes, we sought to investigate whether this process promotes the generation of reactive oxygen species (ROS). Ascorbic acid (Asc) exhibits a maximum absorbance at λ_{max} = 265 nm, and its oxidation leads to a decrease in absorbance at this wavelength.[49] Monitoring ascorbic acid consumption allows us to evaluate the reaction kinetics and determine which complex promotes ascorbic acid oxidation more effectively.

To ensure that no Asc auto-oxidation was occurring, the signal was monitored for 5 min, and then the tested substances were added. In the presence of free Cu(II) ions, a gradual decrease in absorbance is observed, with the reaction reaching completion after approximately 11 minutes (Fig. 4). Significant changes are observed when the reaction involves Cu(II) complexes. The rate of Asc consumption decreases for both complexes in comparison to uncomplexed Cu(II) ions. However, this serves only as a control, as free Cu(II) ions are not typically present in biological systems. For the **CuS4** complex, the reaction is completed within thirteen minutes, while the **CuS5** complex achieves complete reaction in fourteen minutes (Fig. 4).

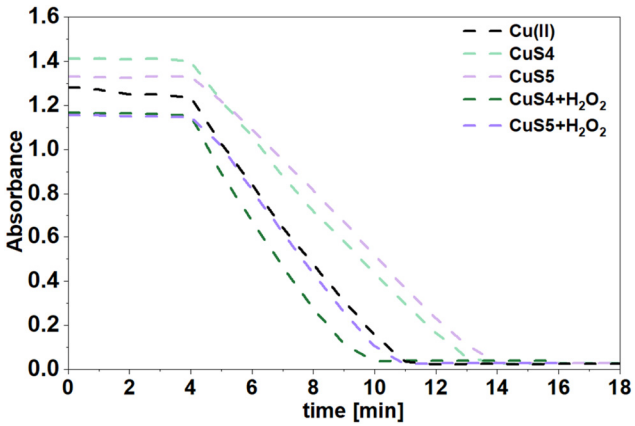

Fig. 4 Ascorbate consumption by **CuS4** and **CuS5** complexes with/without H_2O_2 and uncomplexed Cu(II) ions at pH 6.7 measured by UV spectroscopy (λ = 265 nm) as a function of the time.

When hydrogen peroxide (H_2O_2) is added to the reactions, significant acceleration of the process is observed. For **CuS4** + H_2O_2, the reaction reaches completion in approximately ten minutes, while for the **CuS5** + H_2O_2 in eleven minutes (Fig. 4). The accelerating effect of H_2O_2 on the reaction of complexes with Asc was also observed for other spike protein fragment complexes studied by us previously,[38] namely Cu(II)-Ac-ELDKYFKNH-NH_2 (**CuS1**) and Cu(II)-Ac-WSHPQFEK-NH_2 (**CuS2**). However, the rates of ascorbic acid oxidation for these complexes cannot be directly compared, as different compound concentrations were used in the respective experiments.

Overall, the analysis indicates that both complexes are capable of consuming ascorbic acid and generating reactive oxygen species. Furthermore, the presence of hydrogen peroxide significantly accelerates the generation of ROS. The **CuS4** complex in the presence of hydrogen peroxide exhibits the strongest oxidizing properties towards ascorbic acid, more potent than free Cu(II) ions. This indicates that the **CuS4** complex in the presence of Asc and H_2O_2 appears to exhibit slightly higher ROS generating activity than the **CuS5** complex.

Rhodamine 6G (R6G) degradation. The previous experiment confirmed ROS production by the studied complexes, therefore, in the next step, we decided to investigate whether the hydroxyl radicals ($^{\bullet}OH$) is one of the types of ROS produced by **CuS4** and **CuS5** complexes at pH 6.7. Specifically, we aimed to assess the activity of the complexes in the presence of hydrogen peroxide (H_2O_2) and ascorbic acid (Asc), determine whether either reducing agent can initiate $^{\bullet}OH$ production, and establish which of these molecules is more effective at promoting hydroxyl radical formation in biological systems.

To monitor $^{\bullet}OH$ generation, rhodamine 6G (R6G) was employed as a probe. This dye undergoes degradation in the presence of hydroxyl radicals, which is reflected in a decrease in its maximum absorbance band at λ_{max} = 526 nm.[50] To

Table 2 Summary of the probable reduction of Cu(II) ions in the complexes at pH 6.7 after the addition of ascorbic acid (estimated from the EPR spectra)

	% of Cu(II) ions that were probably reduced by the addition of Asc	
Complex	Immediately after the addition of Asc	After 1 h
CuS4	~50	~70
CuS5	~85	100

compare the ability of the **CuS4** and **CuS5** complexes to produce hydroxyl radicals, the kinetic curves of R6G degradation were plotted (Fig. 5). The kinetic profiles demonstrate that in the control reactions (R6G alone, uncomplexed Cu(II) ions), no $^{\bullet}OH$ generation is observed (Fig. S6). A similar outcome was obtained for the ligand systems, indicating that the **S4** and **S5** ligands do not produce hydroxyl radicals, even in the presence of H_2O_2 (Fig. S6 and Fig. 5A). A moderate decrease in absorbance at 526 nm was noted for R6G incubated with H_2O_2 alone, consistent with its partial degradation under oxidative conditions (Fig. 5A). In the case of uncomplexed Cu(II) ions, the reaction resembles a Fenton-type process, generating hydroxyl radicals (Fig. 5A). However, as previously noted, free Cu(II) ions do not exist in this form under physiological conditions. In the absence of H_2O_2, the complexes do not generate free radicals (Fig. S6). By contrast, significant R6G degradation was observed for both **CuS4** and **CuS5** complexes in the presence of H_2O_2 (Fig. 5C), confirming their ability to produce hydroxyl radicals. Overall, the results suggest that both complexes generate $^{\bullet}OH$ at comparable levels. The **CuS1** and **CuS2** complexes (which we studied before) in the presence of H_2O_2 were found to be slightly more efficient in producing $^{\bullet}OH$ than the **CuS4** and **CuS5** complexes.[38]

Similar measurements were carried out for the compounds in the presence of ascorbic acid (Asc). The absence of a significant decrease in the R6G absorbance band at λ_{max} = 526 nm for R6G, R6G with Asc, or Cu(II) ions without Asc indicates that no hydroxyl radical is generated under these conditions (Fig. S7 and Fig. 5B). The kinetic curves obtained for **S4** and **S5** ligands and their complexes without Asc further confirm that they are incapable of producing $^{\bullet}OH$ (Fig. S7). In contrast, the most pronounced decrease in absorbance was observed for R6G with Cu(II) ions and Asc, followed by R6G with the **CuS4** and **CuS5** complexes and Asc (Fig. 5D), consistent with the results obtained using H_2O_2. For the **CuS4** and **CuS5** complexes with Asc, the extent of absorbance decrease after one hour was comparable, making it difficult to unequivocally determine which complex produces a greater amount of hydroxyl radicals. A similar trend was observed in the R6G + H_2O_2 experiments. Moreover, both complexes produce similar amounts of hydroxyl radicals in the presence of H_2O_2 and Asc.

Owing to the linearity of the kinetic curves within the first five minutes of the reaction, pseudo-first order rate constants (k [min^{-1}]) for hydroxyl radical generation were determined for the studied systems (Table S6). Analysis of the collected data shows that the highest k values were obtained for unbound Cu (II) ions and for both complexes in the presence of Asc, all of which are of the same order of magnitude. The rate constants for the complexes with Asc are very similar $(1.60(3) \times 10^{-2}$ min^{-1} for **CuS5** and $1.40(2) \times 10^{-2}$ min^{-1} for **CuS4**).

An additional experiment was performed to evaluate the ability of DMSO to quench $^{\bullet}OH$ radicals generated by the complexes in the presence of H_2O_2 or Asc. Dimethyl sulfoxide (DMSO) is a well-established hydroxyl radical scavenger.[51] The R6G spectra were registered for the complexes in the presence of H_2O_2 or Asc and DMSO. As expected, no decrease in the

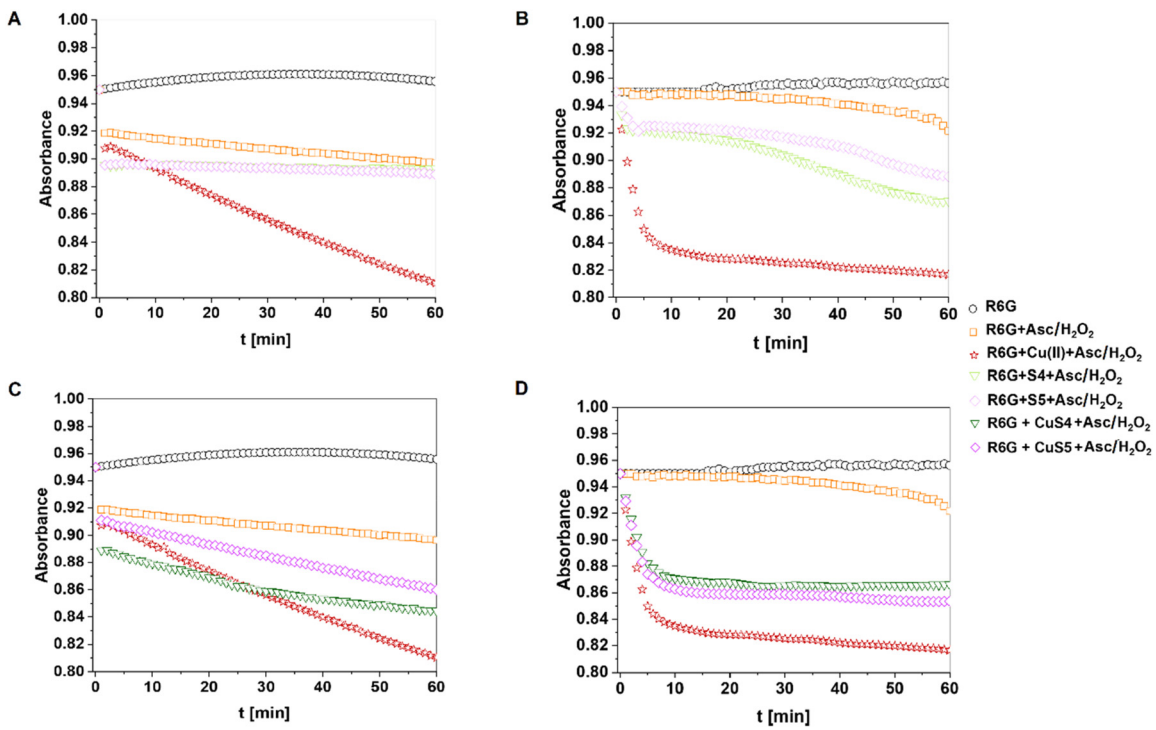

Fig. 5 The experimental kinetic curves of R6G degradation at pH 6.7 in the presence of ligands with (A) H_2O_2 and (B) Asc as well as their corresponding complexes with (C) H_2O_2 and (D) with Asc.

maximum absorption band at 526 nm was observed for R6G in any of the spectra, proving that DMSO efficiently prevents the formation of $^{\bullet}OH$ (Fig. S8 and S9). These findings provide further confirmation that the studied Cu(II) peptide complexes are indeed responsible for hydroxyl radical generation in the presence of reducing agent.

Gel electrophoresis with H_2O_2 and Asc. Experiments conducted using UV-Vis spectroscopy confirmed the generation of hydroxyl radicals by the studied complexes. In turn, gel electrophoresis technique was used to determine whether the **CuS4** and **CuS5** systems at pH 6.7 can also generate other types of ROS and what their impact on plasmid DNA is.

Examination of the lanes corresponding to **CuS4** and **CuS5** complexes without a reducing agent (Fig. 6A1 and A2, lanes 7 and 12, respectively) revealed the formation of II and III forms of DNA, with the native form present in only trace amounts for the **CuS4** complex. Upon addition of H_2O_2, DNA damage was significantly increased, with approximately 70% of linear form of DNA (slightly higher for **CuS4**) and the remaining ~30% of circular form (Fig. 6A1 and B1, lanes 8 and 13). This suggests that both complexes produce massive amounts of ROS, which are highly aggressive toward plasmid DNA. Comparing the reactions of the **CuS4** and **CuS5** complexes with H_2O_2 to those of the Cu(II)-Ac-ELDKYFKNH-NH_2 (**CuS1**) and Cu(II)-Ac-WSHPQFEK-NH_2 (**CuS2**) complexes with different spike

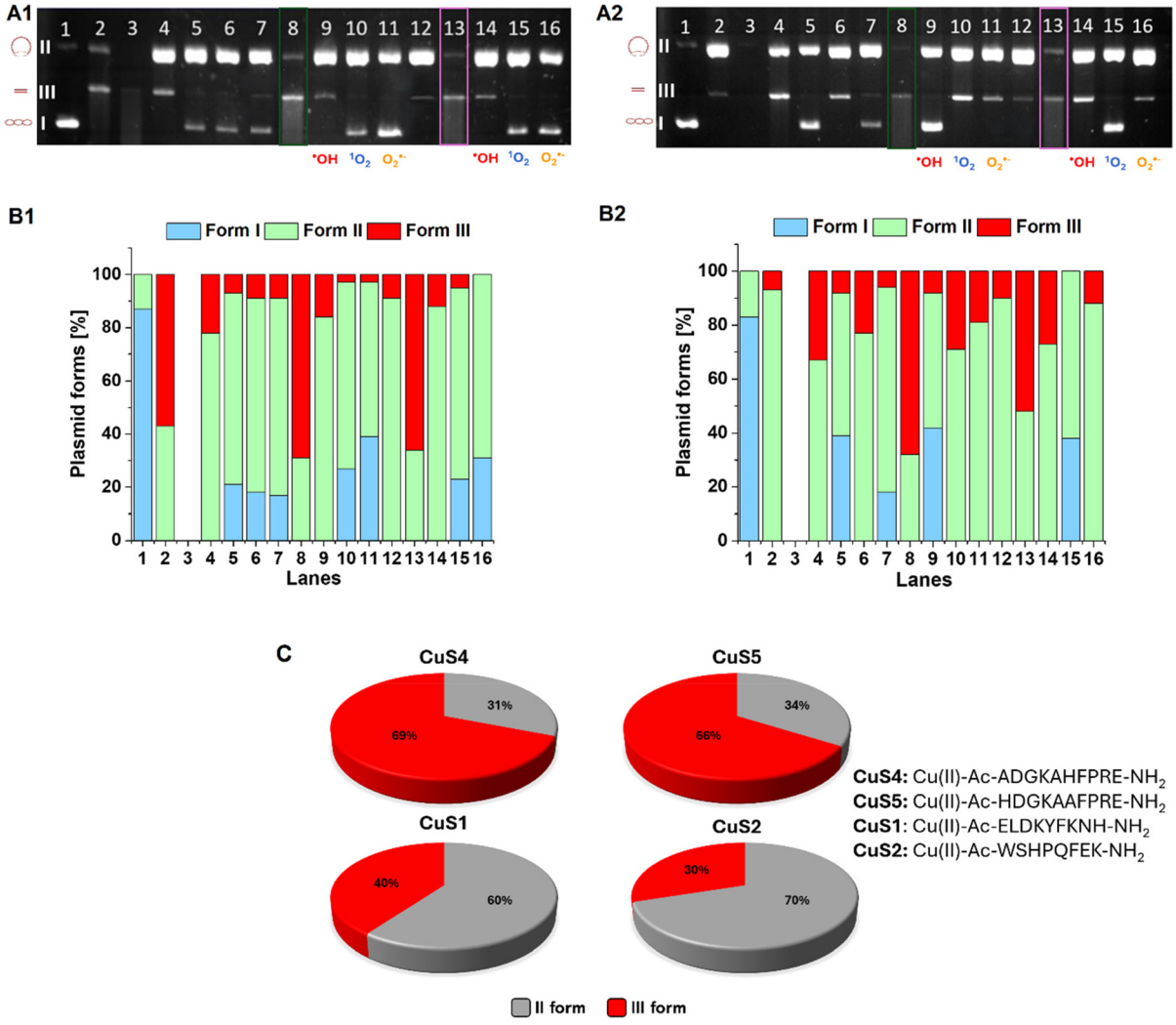

Fig. 6 pBR322 plasmid damage by unbound Cu(II) ions, **S4**, **S5** ligands and **CuS4** and **CuS5** complexes (C = 50 μM) in the presence of (A1) H_2O_2 (C = 50 μM) or (A2) Asc (C = 50 μM) at pH 6.7. Lanes: 1: plasmid; 2: plasmid + Cu(II); 3: plasmid + Cu(II) + H_2O_2/Asc; 4: plasmid + Cu(II) + H_2O_2/Asc + DMSO; 5: plasmid + Cu(II) + H_2O_2/Asc + NaN_3; 6: plasmid + Cu(II) + H_2O_2/Asc + KI; 7: plasmid + **CuS4**; 8: plasmid + **CuS4** + H_2O_2/Asc; 9: plasmid + **CuS4** + H_2O_2/Asc + DMSO; 10: plasmid + **CuS4** + H_2O_2/Asc + NaN_3; 11: plasmid + **CuS4** + H_2O_2/Asc + KI; 12: plasmid + **CuS5**; 13: plasmid + **CuS5** + H_2O_2/Asc; 14: plasmid + **CuS5** + H_2O_2/Asc + DMSO; 15: plasmid + **CuS5** + H_2O_2/Asc + NaN_3; 16: plasmid + **CuS5** + H_2O_2/Asc + KI. (B1) Densitometric analysis of the electropherogram A1 (with H_2O_2), while (B2) for A2 (with Asc) (no DNA form was assigned to lane 3 because the DNA was cut into small pieces) and (C) percentage of form II and form III DNA created by the reaction of Cu(II) complexes with spike protein fragments (**S1**: Ac-ELDKYFKNH-NH_2,[38] **S2**: Ac-WSHPQFEK-NH_2,[38] **S4**: Ac-ADGKAHFPRE-NH_2, **S5**: Ac-HDGKAAFPRE-NH_2) in the presence of H_2O_2.

protein fragments reveal dramatic differences. The **CuS1** system caused to formation of 40% of linear and 60% of circular form of DNA, while the **CuS2** system 30% of form III and 70% of form II of DNA (Fig. 6C).[38] These results demonstrate the huge potential of the systems studied in this paper to generate ROS and damage DNA. The native form of DNA was absent in all tested samples (Fig. 6A1 and B1, lanes 8 and 13). Moreover, trails were observed, indicating further cleavage of DNA into smaller fragments, which reflects extensive DNA damage in these solutions. Lanes 9–11 for the **CuS4** complex and 14–16 for the **CuS5** complex (Fig. 6A1) correspond to solutions containing H_2O_2 and ROS scavengers (DMSO for $^{\bullet}OH$, NaN_3 for $^1O_2$, and KI for $O_2^{\bullet-}$), respectively. The results indicate that **CuS4** and **CuS5** in the presence of H_2O_2, are capable of generating hydroxyl radicals, singlet oxygen, and superoxide anion radicals (Fig. 6A1).

In addition, a control electropherogram (Fig. S10) was prepared for **S4** and **S5** ligands with/without hydrogen peroxide, which showed that none of the tested compounds generate ROS with/without H_2O_2 and, consequently, no DNA damage occurs.

Given that **CuS4** and **CuS5** complexes produce ROS in the presence of H_2O_2, leading to DNA damage, we next performed a similar experiment using ascorbic acid. Comparing the results for both complexes in the presence of ascorbic acid (Fig. 6A2 and B2, lanes 8 and 13 for **CuS4** and **CuS5**, respectively), it is evident that the circular and linear form of DNA are present in similar proportions for **CuS5**, whereas in the **CuS4** system the linear form predominates (approximately 65%). This suggests that ROS generation is more efficient for the **CuS4** complex in the presence of ascorbic acid. The greater activity of the **CuS4** system in causing DNA damage may result from the production of higher concentrations of various ROS compared to the **CuS5** complex. The presence of the three types of ROS mentioned above was also confirmed in this experiment. The differences between the amount of ROS generated by the complexes in this experiment and the lack of differences between them in the R6G degradation test may be due to the fact that rhodamine 6G detects only the hydroxyl radicals. Therefore, the complexes may produce $^{\bullet}OH$ at comparable levels, but other ROS may dominate for the **CuS4** complex, making it more aggressive towards DNA.

A control electropherogram was also prepared for the ligands with and without ascorbic acid (Fig. S11). As in the previous experiments, analysis of the data revealed no detectable plasmid damage upon addition of the ligands. A slight increase in the intensity of the band corresponding to circular form of DNA was observed for both ligands in the presence of ascorbic acid, suggesting that addition of reducing agent causes minimal DNA damage.

The effects of uncomplexed Cu(II) ions and **CuS4** and **CuS5** complexes, in the absence of ascorbic acid or hydrogen peroxide, on plasmid DNA were also examined (Fig. S12). For both complexes (lane 6 for **CuS4** and lane 10 for **CuS5**), a strong band corresponding to II form of DNA and a weaker band corresponding to linear form of DNA were observed, indicating that both complexes are capable of inducing DNA damage even without Asc or H_2O_2. In the case of the **CuS4** complex, the native form of DNA remained detectable. The addition of quenchers to these complexes resulted in the scavenging of small amounts of ROS (Fig. S12, lanes 7–9 and 11–13 for **CuS4** and **CuS5**, respectively). This means that both complexes also have the potential to generate low levels of ROS without the addition of reducing agents.

Peptide oxidation. Given that the ROS generated by studied complexes are capable of inducing DNA oxidation, we next examined whether they can also oxidize amino acid residues within the studied fragments. The oxidation of the **S4** and **S5** peptides was investigated at pH 6.7 by the Cu(II)-H_2O_2 system both in the presence and absence of ascorbic acid. The effect of ascorbic acid itself was also studied on the **CuS4** and **CuS5** complexes.

In contrast to our earlier studies,[52] the oxidation of peptides occurred intensively without hydrogen peroxide. The extent of oxidation was much higher for the **S5** ligand than for **S4**. This difference can be explained by the distinct coordination modes. In the case of the **CuS5** system the formation of the seven-membered ring with the involvement of the imidazole nitrogen of the histidyl residue is less favored, therefore the formation of the adduct between the **S5** ligand and ascorbic acid due to a Diels–Alder reaction between the histidyl residue and the ascorbic acid is more favorable. The presence of this adduct promotes peptides oxidation.[52] In the presence of ascorbic acid, singly and doubly oxidized products are formed, whereas in the absence of ascorbic acid only one product can be identified. Surprisingly, LC-MS measurements revealed that these products in the presence and absence of ascorbic acid are different.

The quantitative evaluation of the systems is complicated by the fact that peptide oxidation also occurs during the ESI-MS measurements. However, these products appear at the same retention time as the ligands, whereas the retention times of the real oxidation products significantly differ from those of the ligands.

Since the molecular formulae of the two peptides are identical, the calculated m/z values of the singly, doubly and triply charged peptides are the same: 1168.586, 584.797 and 390.200 m/z, respectively. The **S4** ligand elutes at 11.7 min, while the **S5** peptide elutes at 11.6 min during the HPLC measurements.

Because of the similarity of these peptides, the results are presented only for the **S5** ligand. The chromatograms of the studied **S5** peptide systems are shown in Fig. 7. The main peak is slightly split in systems containing ascorbic acid. The LC-ESI-MS spectra of the main peak (11.3–12.1 min) in the Cu(II) : **S5** : H_2O_2 : Asc = 1 : 1 : 4 : 20 system are presented in Fig. S16. The first half of the peak corresponds to the peptide, the second part is the singly oxidized peptide with 592.791 m/z value (calculated value is 592.794 m/z), as can be seen on the extracted ion chromatograms (Fig. S17). The doubly oxidized peptide appears at a lower retention time with 600.788 m/z (calculated value is 600.791 m/z). The second green peak is also the doubly oxidized peptide, but it is formed only during

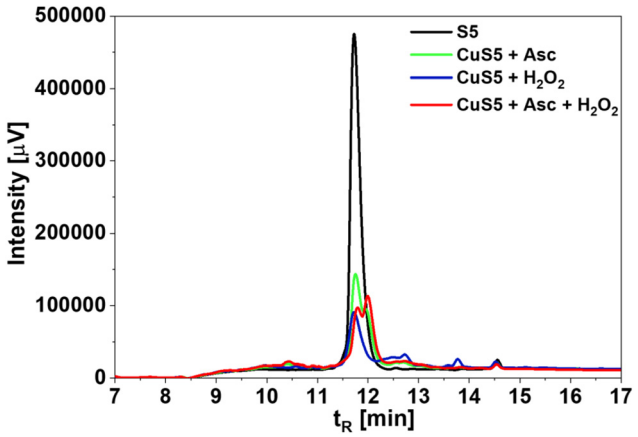

Fig. 7 HPLC chromatograms of the **S5** peptide at pH 6.7 and its oxidation products formed in the different studied systems during 60 min of oxidation.

the ESI-MS measurements. The products are the same in the Cu(II) : peptide : Asc = 1 : 1 : 20 and in the Cu(II) : peptide : H_2O_2 : Asc = 1 : 1 : 4 : 20 systems, the only difference is their ratio and in the presence of hydrogen peroxide the extent of oxidation is higher, as expected.

Oxidation occurs at the histidyl residue, and this is demonstrated, as a representative example, by the fragmentation of the oxidized **S4** peptide in the Cu(II) : **S4** : H_2O_2 : Asc = 1 : 1 : 4 : 20 system (Fig. 8A). This process is less pronounced in the case of the **S5** peptide, as the histidyl residue is located at the first position, and fragmentation initiates at the *N*-terminus. By the loss of the Ac-Ala moiety of the peptide, the remaining fragment is still oxidized in the case of the **S4** peptide, and the $[DGKAHFPRE\text{-}NH_2 + O]^{2+}$ ion appears with 536.272 *m*/*z* value (Fig. 8A). The $[GKAHFPRE\text{-}NH_2 + O]^{2+}$ and $[KAHFPRE\text{-}NH_2 + O]^{2+}$ ions are also present with 478.759 and 450.251 *m*/*z* values, respectively, while following the loss of the lysyl residue, the resulting ion is only singly charged (Fig. 8A). It is $[AHFPRE\text{-}NH_2 + O]^{+}$ with 771.378 *m*/*z*. $[HFPRE\text{-}NH_2 + O]^{+}$ with 700.344 *m*/*z* is also present, on the other hand, by the loss of the histidyl residue $[FPRE\text{-}NH_2 + O]^{+}$ with 563.294 *m*/*z* is not present, only $[FPRE\text{-}NH_2]^{+}$ with 547.294 *m*/*z* can be identified (Fig. 8A). This supports the conclusion that peptide oxidation occurs at the histidyl residue. Oxidation of the histidyl residue may initiate *via* attack by a hydroxyl radical at the

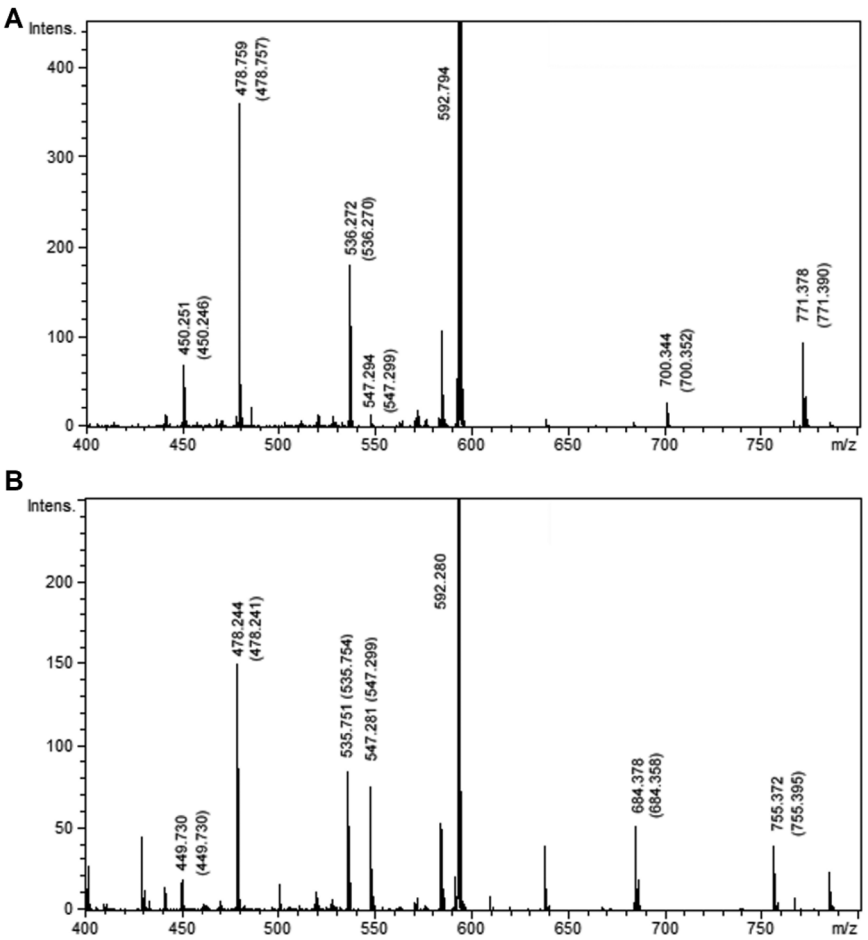

Fig. 8 ESI-MS/MS spectra of the singly oxidized products of the **S4** peptide formed in the: (A) Cu(II) : **S4** : H_2O_2 : Asc = 1 : 1 : 4 : 20 and (B) Cu(II) : **S4** : H_2O_2 = 1 : 1 : 4 systems (*m*/*z* values in parenthesis are the calculated ones).

C2 position, forming 2-oxo-His (Scheme 1). Reaction of a hydroxyl radical at the C4 or C5 positions requires rearrangement *via* reversible water elimination and subsequent radical addition to yield 2-oxo-His. Otherwise, fragmentation of the imidazole ring would occur,[53] which is not supported by our results.

However, in the case of the Cu(II) : peptide : H_2O_2 = 1 : 1 : 4 systems, the doubly charged product has 592.280 *m*/*z* value, which is 0.5 *m*/*z* smaller than the singly oxidized product in the presence of ascorbic acid. If it is caused only by the loss of a hydrogen atom of a singly oxidized peptide, this value should be 592.290 *m*/*z*. If the product is doubly oxidized, the elimination of an $-NH_3$ group would result in 592.278 *m*/*z*. This value is closer to the measured one, and the ESI-MS/MS measurements supported this suggestion: the lysine side chain is doubly oxidized, and this process is accompanied by the loss of ammonia. Consequently, the lysyl side chain undergoes deamination and oxidation, resulting in the formation of α-aminoadipic acid (see Scheme 2).

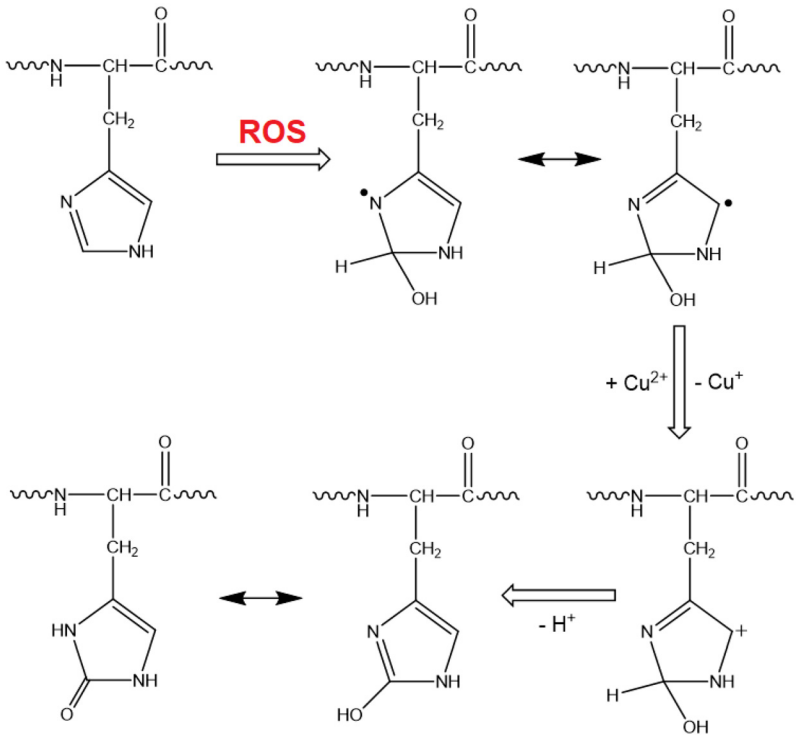

Scheme 1 Oxidation of the histidyl residue.

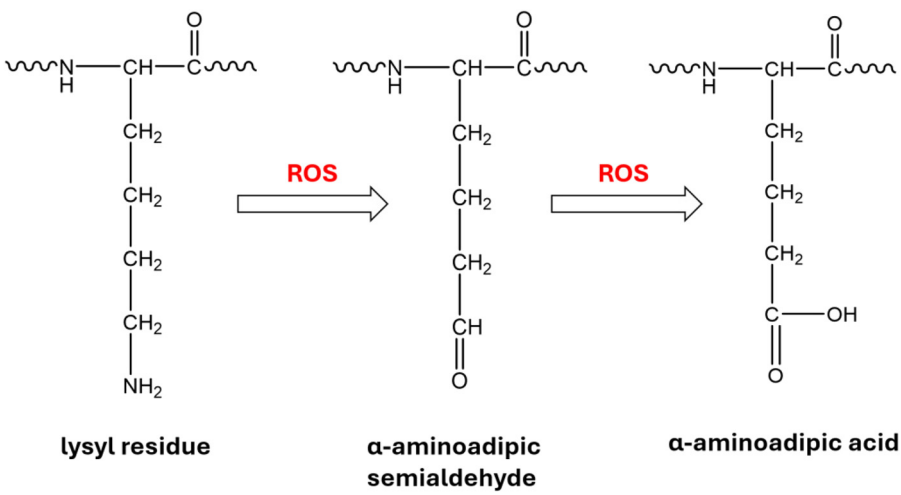

Scheme 2 Two-step oxidation of the lysyl residue.

This process has been reported in the literature,[54,55] although it was not observed in our previous studies. However, under the experimental conditions applied in the present work, the formation of α-aminoadipic acid was clearly demonstrated. Notably, studies reported in the literature have shown that α-aminoadipic acid concentration is significantly elevated in the serum (this metabolite can be released from tissues into the circulation) of COVID-19 patients compared with control groups, and it has even been proposed as a potential biomarker of COVID-19 disease.[25] Importantly, α-aminoadipic acid has also been identified as a biomarker in pathological conditions associated with high morbidity and mortality, including aging, sepsis, and renal failure.[25] Furthermore, the formation of α-aminoadipic acid promotes pro-oxidative conditions by enhancing ROS generation, leading to lipid peroxidation and protein oxidation. *a*-aminoadipic acid has been shown to interfere with trypsin secretion, resulting in impaired pancreatic function,[56] and has been associated with diabetes,[57] dysregulation of glutamatergic neurotransmission,[58] atherosclerosis, and inflammation.[59] Therefore, the formation of α-aminoadipic acid in the studied systems suggests a potential risk to biological systems and justifies the need for further investigation.

The fragmentation of the oxidized product also begins at the *N*-terminus, by the loss of the Ac-Ala moiety of the peptide. The remaining fragment is still doubly oxidized and the $[DGKAHFPRE\text{-}NH_2 - NH_3 + 2O]^{2+}$ ion appears at 535.751 *m*/*z* value (Fig. 8B). Successive losses of the aspartic and glycyl residues yield the $[GKAHFPRE\text{-}NH_2 - NH_3 + 2O]^{2+}$ and $[KAHFPRE\text{-}NH_2 - NH_3 + 2O]^{2+}$ ions with 478.244 and 449.730 *m*/*z* values, respectively (Fig. 8B). By the loss of the lysyl site, two oxygen atoms also leave and the resulting ion is singly charged ($[AHFPRE\text{-}NH_2]^+$ with 755.372 *m*/z, Fig. 8B). This ion together with the $[HFPRE\text{-}NH_2]^+$ ion at 684.378 *m*/*z* unambiguously confirms that the histidine residue is not oxidized in this case, while $[FPRE\text{-}NH_2]^+$ ion with 547.281 *m*/*z* is identical to that formed in the presence of ascorbic acid (Fig. 8B).

Conclusions

This paper describes the ability of essential (copper, iron, manganese, cobalt, and zinc) and potentially essential (nickel) metal ions to coordinate two modified fragments (Ac-ADGKAHFPRE-NH_2, **S4** and Ac-HDGKAAFPRE-NH_2, **S5**) of the SARS-CoV-2 spike protein. Apart from this aspect, the article focuses on the analysis of the redox activity of both complexes and their ability to produce reactive oxygen species (ROS) that damage DNA and participate in metal-catalyzed peptide oxidation.

We demonstrated that Cu(II) ions, whose elevated concentrations were found in COVID-19 patients, are most effective in forming Cu(II) complexes with the studied spike protein fragments than other studied metal ions. The 3N complex $\{N_{im}, 2N^-\}$ dominates for the **S4** peptide in the lung environment (pH 6.7). In turn, for the **S5** ligand, a mixture of two species was observed at lung pH with $1N\{N_{im}\}$ and $2N\{N_{im}, N^-\}$ coordination modes.

Furthermore, we confirmed that Cu(II) ions in both complexes can cyclize between Cu(II)/Cu(I) oxidation states. Addition of ascorbic acid to the complexes leads to the reduction of Cu(II) ions to Cu(I) ions. This ability to redox cycle of Cu ions leads to the generation of reactive oxygen species (ROS) by the **CuS4** and **CuS5** complexes. Addition of hydrogen peroxide to both compounds accelerated the oxidation of ascorbic acid. The rhodamine 6G degradation experiment demonstrated that both complexes are capable of generating similar levels of hydroxyl radical. The **CuS1** and **CuS2** complexes in the presence of H_2O_2 were found to be slightly more efficient in producing $^{\bullet}OH$ than the **CuS4** and **CuS5** complexes. Other types of ROS ($O_2^{\bullet -}$ and $^1O_2$) were also identified as those produced by the tested complexes. Both compounds produce ROS which induce the formation of circular and linear form of DNA. What is interesting is that ROS generated by **CuS4** and **CuS5** in the presence of H_2O_2 cause greater DNA damage than those generated by the **CuS1** and **CuS2** complexes.

Moreover, our studies on peptide oxidation demonstrated that both peptides undergo oxidative modification. However, the oxidation pathway differs depending on whether the reaction is carried out in the Cu(II)/H_2O_2 system alone or in the presence of ascorbic acid. In the absence of ascorbic acid, oxidation occurs primarily at the lysyl residue, leading to the formation of a doubly oxidized product at the lysine site, identified as α-aminoadipic acid. In contrast, the presence of ascorbic acid promotes oxidation at the histidyl residue. Our results indicate that Cu(II) ions play a key role in the complexation of the spike protein and may profoundly influence its capacity to produce ROS. This process may exert detrimental effects on cellular DNA and proteins, thereby adversely affecting patient health.

Furthermore, our findings demonstrate that selective oxidation of specific amino acid residues within peptides can be achieved in a controlled manner to elicit defined outcomes. Such an approach has significant implications for studies aimed at modulating oxidative stress, elucidating the cellular consequences of site-specific amino acid oxidation, or preventing the formation of particular oxidized products. In our case, the formation of α-aminoadipic acid is particularly relevant, as it may further exacerbate the pro-oxidative environment induced by the Cu(II)-spike protein fragment, thereby amplifying ROS generation, lipid peroxidation, and downstream pathogenic cellular effects.

Experimental section

Coordination studies

Potentiometric measurements. The stability constants for **S4**, **S5** peptides and their Cu(II) complexes (**CuS4**, **CuS5**) were calculated from pH-metric titrations performed on a MOLSPIN pH-meter system with an ERH-13-6 electrode. The pH readings were converted into hydrogen ion concentration as described

earlier.[60] The experiments were carried out at 298 K under an argon atmosphere using a total sample volume of 2 mL. As the titrant, CO_2-free, 0.1024 M NaOH was used. The Cu(II) stock solution was prepared from $Cu(NO_3)_2 \times 3H_2O$. The ligand concentration was 0.002 M, and the metal to ligand molar ratios for the studied complexes were 1 : 1 (the concentration of the stock solution of Cu(II) ions was 0.05 M). All measurements were carried out at a constant ionic strength of 0.1 M KNO_3. Samples were prepared in distilled water (Simplicity UV, Millipore, 18.2 MΩ resistance) in the presence of HNO_3 to obtain an acidic pH. The samples were titrated twice in the pH range 2.5–10.5. The final results were calculated with SUPERQUAD[61] and HYPERQUAD[62] software. The results of the ligand's titration in the presence of Cu(II) ions were analyzed in batch calculations, in which all titration curves were fitted at the same time with one model. The standard deviation values were referred to random errors only. The purity and the exact concentration of the ligand solutions were determined by the Gran method.[63] The equilibrium reactions of the ligands with protons and Cu(II) ions are given in the eqn (1):

$$pCu + qH + rL = Cu_pH_qL_r, \quad (1)$$

where L stands for the studied peptide. The stability constant, β_{pqr}, is defined by eqn (2):

$$\beta_{pqr} = [Cu_pH_qL_r]/[Cu]^p[H]^q[L]^r. \quad (2)$$

Analogous experiments to those performed with Cu(II) ions were conducted for the **S4** and **S5** ligands using other transition metal ions, namely Zn(II), Mn(II), Fe(III), Fe(II), Ni(II), and Co(II). It is worth emphasizing that Mohr's salt was used as the source of Fe(II) ions. Due to the high sensitivity of Fe(II) ions to oxidation, all reagents were purged with argon prior to solution preparation. The sample volume was 3 mL, with a ligand concentration of 1 mM and a 1 : 1 metal to ligand molar ratio, at an ionic strength of 0.2 M KCl. CO_2-free 0.1937 M NaOH was used as the titrant. Potentiometric titrations were carried out using a MOLSPIN pH meter equipped with a Metrohm 6.0234.100 combined glass electrode. The protonation constants of the ligands and the overall stability constants of the complexes were determined using the SUPERQUAD[61] and the PSEQUAD software, respectively.[64]

Spectroscopic techniques. The concentrations of the studied solutions were similar to those used in potentiometric studies. The metal to ligand molar ratio was 1 : 1. The complexes were measured in the pH range of 3.0–11.0 in 1 and 0.1 cm cuvettes. NaOH and HNO_3 solutions were used to adjust the pH value. The electron absorption (UV-Vis) spectra were recorded on a Cary 60 spectrophotometer (Agilent Technologies) over the spectral range of 200–900 nm, while the circular dichroism (CD) spectra were recorded on a J-715 spectropolarimeter (JASCO) in the range of 200–800 nm. The spectra are expressed in terms of $\Delta\varepsilon = \varepsilon_L - \varepsilon_R$, where ε_L and ε_R are the molar absorption coefficients for left and right circularly polarized light, respectively. The electron paramagnetic resonance (EPR) spectra of Cu(II) complexes were measured on a Bruker spectrometer (Bruker ELEXSYS E500 CW-EPR) at an X-band frequency (9.45 GHz). A solution of ethylene glycol in water was added to each sample (3 : 10, v:v) to obtain a glass forming solvent upon freezing with liquid nitrogen. The measurements were carried out at 77 K. The experimental spectra were computer-simulated with Bruker WinEPR SimFonia software.

ESI-MS measurements. The mass spectra were recorded on a Bruker MicrOTOF-Q spectrometer (Bruker Daltonik, Bremen, Germany), equipped with Apollo II electrospray ionization source. The following instrumental parameters were set: scanning range 0–2500 *m*/*z*, temperature 200 °C, dry gas-nitrogen, reflector voltage 1300 V, detector voltage 1920 V. The mass spectrometer was operated in positive ion mode. All studied samples were prepared in water at pH about 7.0. The spectra were measured for the complexes (in 1 : 1 metal to ligand molar ratio) and infused at a flow rate of 3 μL min^{-1}. The instrument was calibrated externally with the Tunemix™ mixture (Bruker Daltonik, Germany) in the quadratic regression mode.

Redox activity

Electrochemical measurements. Cyclic voltammetry measurements for **S4** and **S5** ligands (1 mM) as well as for their Cu(II) complexes (**CuS4** and **CuS5**) (1 : 5 M : L molar ratio, [L] = 1 mM) were carried out at room temperature by a BASi Epsilon EC potentiostat. A standard system containing three electrodes was applied: (1) glassy carbon electrode (GCE) as a working electrode (diameter 3 mm), (2) BASi SEC-C Pt counter electrode (platinum wire), and (3) reference electrode (BASi MF-2052 Ag/AgCl electrode). All measurements were carried out in water solutions using 0.2 M KNO_3 as the supporting electrolyte in the selected potential window from −0.6 to 0.8 V *vs.* Ag/AgCl under an N_2 atmosphere. The measurements were performed with different scan rates: 25, 50, 100 and 200 mV s^{-1}.

Reduction of Cu(II) ion by Asc. In the experiment concerning the reduction of the Cu(II) ion in the complex (C = 1 mM) after the addition of ascorbic acid (C = 1 mM), EPR spectra were measured using a Bruker Elexsys E500 spectrometer operating at a frequency of about 9.6 GHz (X band). The reactions were carried out in sealed glass capillaries. The experimental spectrum was simulated by using Bruker WinEPR SimFonia software.

ROS formation

Ascorbic acid consumption test. The UV-Vis spectra of ascorbic acid consumption were monitored by the decrease in the maximum absorption band at 265 nm (145 000 M^{-1} cm^{-1}).[49] The spectra were recorded as a function of time on a Cary 60 spectrophotometer at 25 °C. All samples were prepared in phosphate-buffered saline (PBS) at pH 6.7 containing ligand (C = 12 μM), Cu(II) ions (C = 10 μM) and ascorbic acid (C = 100 μM) with/without hydrogen peroxide (C = 50 μM). Each reaction was repeated three times.

Rhodamine 6G degradation. The hydroxyl radical ($^{\bullet}OH$) generation by uncomplexed Cu(II) ions, **S4**, **S5** ligands and

their **CuS4**, **CuS5** complexes at the pH 6.7 in the presence of H_2O_2 or Asc was studied in rhodamine 6G degradation (R6G) assay by UV-Vis spectroscopy. The following concentrations: 5 μM of R6G, 50 μM of **S4**, **S5** ligands, 50 μM of **CuS4**, **CuS5** complexes (1 : 1 M : L molar ratio) and 5 mM of H_2O_2 were used in experiments with hydrogen peroxide. In turn in experiment with addition of Asc, the concentrations such as 10 μM of R6G, 100 μM of **S4**, **S5** ligands, 100 μM of **CuS4**, **CuS5** complexes (1 : 1 M : L molar ratio) and 0.380 mM of Asc were used. All experiments were carried out in the presence of PBS buffer. Rhodamine 6G (R6G) was used as a hydroxyl radical detector. If the $^{\bullet}OH$ is produced in the system, it reacts with R6G and causes its degradation. Then, the decrease of the maximum absorption band at 526 nm is observed.[50] Spectrophotometric measurements were carried out over the spectral range of 400–600 nm in a 1 cm cuvette. UV-Vis spectra were recorded with a Cary 60 spectrophotometer (Agilent Technologies).

ROS identification and DNA damage. The ability of the **CuS4** and **CuS5** systems to induce single- or double-strand DNA breaks (final DNA concentration per lane was C = 0.31 μg mL^{-1}) was investigated with the pBR322 plasmid. All substances ([L] = 50 μM, 1 : 1 M : L molar ratio) were dissolved in PBS buffer (at pH 6.7) with/without hydrogen peroxide (H_2O_2, C = 50 μM) or ascorbic acid (Asc, C = 50 μM), potassium iodide (KI, C = 8 mM), dimethyl sulfoxide (DMSO, C = 0.14 M), or sodium azide (NaN_3, C = 40 mM). After 1 h of incubation at 37 °C, the reaction mixtures (20 μL) were mixed with 3 μL of loading buffer (bromophenol blue in 30% glycerol) and loaded on 1% agarose gel, containing ethidium bromide (EB) in TBE buffer (90 mM Tris borate, 20 mM EDTA, pH 7.4). The gel electrophoresis was carried out at a constant voltage of 120 V for 120 min. The gel was photographed and processed using a Digital Imaging System (Syngen Biotech). Densitometric analysis was performed using a GelAnalyzer 19.1.

Peptide oxidation

Samples consisting of **CuS4**/**CuS5** complexes ([L] = 0.6 mM, 1 : 1 M : L molar ratio) were incubated at pH 6.7 in the presence of H_2O_2 (1 : 4 L : H_2O_2 molar ratio), ascorbic acid (Asc) (1 : 20 L : Asc molar ratio), or a mixture of H_2O_2 and Asc (1 : 4 : 20 L : H_2O_2 : Asc molar ratio). Incubations were carried out at room temperature for 60 min. The reaction was initiated by the addition of H_2O_2, Asc, or H_2O_2 + Asc and was stopped by the addition of Na_2EDTA (1 : 5 L : Na_2EDTA molar ratio). The prepared samples were analyzed by analytical reverse-phase high-performance liquid chromatography (RP-HPLC) using a Jasco system equipped with a Jasco MD-2010 Plus multiwavelength detector, monitoring absorbance at 222 nm. Oxidized products were separated on a Teknokroma Europa Protein C_{18} column (250 × 4.6 mm, 300 Å, 5 μm) at a flow rate of 1 mL min^{-1}. Water (A) and acetonitrile (B), both containing 0.1% TFA were used as the mobile phase. The following gradient was applied: 0.0–3.0–5.5–10.0–22.0–27.0–30.0 min, 100–100–85–80–80–100–100% solvent A.

In the next step, MS and MS/MS measurements of the studied samples were carried out in the positive ion mode using a MicroTOF-Q type Qq-TOF MS instrument (Bruker Daltonik, Bremen, Germany). The instrument was equipped with an electrospray ionization (ESI) source operated at a spray voltage of 4 kV, with nitrogen used as the drying gas. The drying gas temperature was set to 200 °C, and the flow rate was 4.0 L min^{-1} (8.0 L min^{-1} for HPLC-MS). For MS/MS experiments, nitrogen was employed as the collision gas, with a collision cell pressure of 1.2×10^{-2} mbar. Precursor ions were isolated using a 5 *m*/*z* window, and MS/MS spectra were acquired with a digitizer operating at a sampling rate of 2 GHz. External calibration of the mass spectra was performed using the exact masses of $[(NaTFA)_n + Na]^+$ cluster ions generated from an electrosprayed sodium trifluoroacetate (NaTFA) solution. Spectral data were processed using DataAnalysis 3.4 software (Bruker). Sample solutions were introduced directly into the ESI source by syringe infusion using a syringe pump (Cole–Parmer Instrument Company, Vernon Hills, IL, USA) at a flow rate of 3 μL min^{-1}, while a flow rate of 10 μL min^{-1} was applied for LC-MS measurements.

Conflicts of interest

There are no conflicts to declare.

Data availability

The data supporting this article can be found in supplementary information (SI). Supplementary information: detailed description of the coordination of Cu(II) ions to the tested peptides in a wide pH range of 2.5–10.5 (without taking into account the pH of the lungs), the formation and deprotonation constants for **S4** and **S5** peptides with appropriate transition metal ions, UV-Vis and CD spectra, cyclic voltammetric profiles, the experimental kinetic curves of R6G, absorption spectra of R6G solutions with addition of DMSO, gel electropherograms, EPR spectra, ESI-MS and LC-ESI-MS spectra, chromatograms. See DOI: **https://doi.org/10.1039/d6qi00236f**.

Acknowledgements

This research was funded by the Polish National Science Centre (grant number 2021/05/X/ST4/00311). The research was supported by Visegrad Fellowship No. [#62320116].

References

1 D. P. Rosanna and C. Salvatore, Reactive oxygen species, inflammation, and lung diseases, *Curr. Pharm. Des.*, 2012, **18**, 3889–3900.
2 C. Michaeloudes, H. Abubakar-Waziri, R. Lakhdar, K. Raby, P. Dixey, I. M. Adcock, S. Mumby, P. K. Bhavsar and K. F. Chung, Molecular mechanisms of oxidative stress in asthma, *Mol. Aspects Med.*, 2022, **85**, 101026.

3 P. J. Barnes, Oxidative Stress in Chronic Obstructive Pulmonary Disease, *Antioxidants*, 2022, **11**, 965.
4 M. Kellner, S. Noonepalle, Q. Lu, A. Srivastava, E. Zemskov and S. M. Black, ROS Signaling in the Pathogenesis of Acute Lung Injury (ALI) and Acute Respiratory Distress Syndrome (ARDS), *Adv. Exp. Med. Biol.*, 2017, **967**, 105–137.
5 E. Y. Lim, S. Y. Lee, H. S. Shin and G. D. Kim, Reactive Oxygen Species and Strategies for Antioxidant Intervention in Acute Respiratory Distress Syndrome, *Antioxidants*, 2023, **12**, 2016.
6 S. Tasaka, F. Amaya, S. Hashimoto and A. Ishizaka, Roles of oxidants and redox signaling in the pathogenesis of acute respiratory distress syndrome, *Antioxid. Redox Signaling*, 2008, **10**, 739–753.
7 E. Filaire, C. Dupuis, G. Galvaing, S. Aubreton, H. Laurent, R. Richard and M. Filaire, Lung cancer: what are the links with oxidative stress, physical activity and nutrition, *Lung Cancer*, 2013, **82**, 383–389.
8 T. Veenith, H. Martin, M. L. Breuilly, T. Whitehouse, F. Gao-Smith, N. Duggal, J. M. Lord, R. Mian, D. Sarphie and P. Moss, High generation of reactive oxygen species from neutrophils in patients with severe COVID-19, *Sci. Rep.*, 2022, **12**, 10484.
9 M. Sosnowska, M. Wierzbicki, B. Nasiłowska, T. N. Bakalova, K. Piotrowska, B. Strojny-Cieślak, E. Sawosz and M. Kutwin, Fullerenol $C_{60}(OH)_{40}$ Nanoparticles and Ectoine Protect Human Nasal Epithelial Cells Against the Cytokine Storm After Addition of the Full-Length Spike Protein from SARS-CoV-2, *Int. J. Nanomed.*, 2024, **19**, 12221–12255.
10 Y. Huang, C. Yang, X. F. Xu, W. Xu and S. W. Liu, Structural and functional properties of SARS-CoV-2 spike protein: potential antivirus drug development for COVID-19, *Acta Pharmacol. Sin.*, 2020, **41**, 1141–1149.
11 J. Y. Youn, Y. Zhang, Y. Wu, M. Cannesson and H. Cai, Therapeutic application of estrogen for COVID-19: Attenuation of SARS-CoV-2 spike protein and IL-6 stimulated, ACE2-dependent NOX2 activation, ROS production and MCP-1 upregulation in endothelial cells, *Redox Biol.*, 2021, **46**, 102099.
12 J. S. Greenberger, W. Hou, D. Shields, R. Fisher, M. W. Epperly, I. Sarkaria, P. Wipf and H. Wang, SARS-CoV-2 Spike Protein Induces Oxidative Stress and Senescence in Mouse and Human Lung, *In Vivo*, 2024, **38**, 1546–1556.
13 T. Barhoumi, B. Alghanem, H. Shaibah, F. A. Mansour, H. S. Alamri, M. A. Akiel, F. Alroqi and M. Boudjelal, SARS-CoV-2 Coronavirus Spike Protein-Induced Apoptosis, Inflammatory, and Oxidative Stress Responses in THP-1-Like-Macrophages: Potential Role of Angiotensin-Converting Enzyme Inhibitor (Perindopril), *Front. Immunol.*, 2021, **12**, 728896.
14 M. A. Zoroddu, J. Aaseth, G. Crisponi, S. Medici, M. Peana and V. M. Nurchi, The essential metals for humans: a brief overview, *J. Inorg. Biochem.*, 2019, **195**, 120–129.
15 C. Andreini, F. Arnesano and A. Rosato, The zinc proteome of SARS-CoV-2, *Metallomics*, 2022, **14**, mfac047.
16 H. M. Habib, S. Ibrahim, A. Zaim and W. H. Ibrahim, The role of iron in the pathogenesis of COVID-19 and possible treatment with lactoferrin and other iron chelators, *Biomed. Pharmacother.*, 2021, **136**, 111228.
17 E. Suriawinata and K. J. Mehta, Iron and iron-related proteins in COVID-19, *Clin. Exp. Med.*, 2023, **23**, 969–991.
18 H. I. Afridi, T. G. Kazi, F. N. Talpur, J. A. Baig, G. Q. Chanihoon, A. Lashari and G. M. Channa, Elemental Concentrations in Biological Samples of Coronavirus Disease (COVID-19) and Other Pulmonary Disease Patients, *Am. J. Anal. Chem.*, 2021, **12**, 162–187.
19 W. T. A. Masoodi, S. W. Radhi, H. K. Al-Hakeim and H. K. Abdalsada, Trace element imbalance as a possible factor in long-COVID pathophysiology: Links to disease duration and inflammation, *Am. J. Med. Sci.*, 2026, **371**, 259–266.
20 A. Ścibior and E. Wnuk, Elements and COVID-19: A Comprehensive Overview of Studies on Their Blood/Urinary Levels and Supplementation with an Update on Clinical Trials, *Biology*, 2022, **11**, 215.
21 B. Aryal, J. Tillotson, K. Ok, A. T. Stoltzfus, S. L. J. Michel and V. A. Rao, Metal-induced oxidative stress and human plasma protein oxidation after SARS-CoV-2 infection, *Sci. Rep.*, 2023, **13**, 2441.
22 S. Khan, M. S. Shafiei, C. Longoria, J. W. Schoggins, R. C. Savani and H. Zaki, SARS-CoV-2 spike protein induces inflammation via TLR2-dependent activation of the NF-κB pathway, *eLife*, 2021, **10**, e68563.
23 R. Ou, G. Aodeng and J. Ai, Advancements in the Application of the Fenton Reaction in the Cancer Microenvironment, *Pharmaceutics*, 2023, **15**, 2337.
24 C. A. Juan, J. M. Pérez de la Lastra, F. J. Plou and E. Pérez-Lebeña, The Chemistry of Reactive Oxygen Species (ROS) Revisited: Outlining Their Role in Biological Macromolecules (DNA, Lipids and Proteins) and Induced Pathologies, *Int. J. Mol. Sci.*, 2021, **22**, 4642.
25 S. Akmese, I. Koyuncu and E. S. Seyhanli, New Biomarkers in the Diagnosis of COVID-19: Amino Acids, *Int. J. Curr. Med. Biol. Sci.*, 2022, **2**, 127–135.
26 D. Azzouz, M. A. Khan and N. Palaniyar, ROS induces NETosis by oxidizing DNA and initiating DNA repair, *Cell Death Discovery*, 2021, **7**, 113.
27 D. A. Pratt, K. A. Tallman and N. A. Porter, Free radical oxidation of polyunsaturated lipids: New mechanistic insights and the development of peroxyl radical clocks, *Acc. Chem. Res.*, 2011, **44**, 458–467.
28 D. Moris, M. Spartalis, E. Spartalis, G. S. Karachaliou, G. I. Karaolanis, G. Tsourouflis, D. I. Tsilimigras, E. Tzatzaki and S. Theocharis, The role of reactive oxygen species in the pathophysiology of cardiovascular diseases and the clinical significance of myocardial redox, *Ann. Transl. Med.*, 2017, **5**, 326.
29 A. Singh, R. Kukreti, L. Saso and S. Kukreti, Oxidative Stress: A Key Modulator in Neurodegenerative Diseases, *Molecules*, 2019, **24**, 1583.

30 E. A. M. Saleh, F. Al-Dolaimy, Y. Q. Almajidi, S. Baymakov, M. M. A. Kader, M. I. Ullah, A. H. R. Abbas, I. H. Khlewee, Y. S. Bisht and A. H. Alsaalamy, Oxidative stress affects the beginning of the growth of cancer cells through a variety of routes, *Pathol., Res. Pract.*, 2023, **249**, 154664.

31 J. S. Bhatti, A. Sehrawat, J. Mishra, I. S. Sidhu, U. Navik, N. Khullar, S. Kumar, G. K. Bhatti and P. H. Reddy, Oxidative stress in the pathophysiology of type 2 diabetes and related complications: Current therapeutics strategies and future perspectives, *Free Radical Biol. Med.*, 2022, **184**, 114–134.

32 S. Yang and G. Lian, ROS and diseases: role in metabolism and energy supply, *Mol. Cell. Biochem.*, 2020, **467**, 1–12. Erratum: S. Yang and G. Lian, ROS and diseases: role in metabolism and energy supply, *Mol. Cell. Biochem.*, 2020, **467**, 13.

33 A. B. Jena, R. R. Samal, N. K. Bhol and A. K. Duttaroy, Cellular Red-Ox system in health and disease: The latest update, *Biomed. Pharmacother.*, 2023, **162**, 114606.

34 V. R. Rajpal, S. Sharma, A. Kumar, S. Vaishnavi, A. Singh, D. Sehgal, M. Tiwari, S. Goel and S. N. Raina, Mapping of SARS-CoV-2 spike protein evolution during first and second waves of COVID-19 infections in India, *Future Virol.*, 2022, **17**, 557–575.

35 Y. Liao, J. Zhao, K. Bulek, F. Tang, X. Chen, G. Cai, S. Jia, P. L. Fox, E. Huang, T. T. Pizarro, M. F. Kalady, M. W. Jackson, S. Bao, G. C. Sen, G. R. Stark, C. J. Chang and X. Li, Inflammation mobilizes copper metabolism to promote colon tumorigenesis via an IL-17-STEAP4-XIAP axis, *Nat. Commun.*, 2020, **11**, 900.

36 C. Jiang, B. Wu, M. Xue, J. Lin, Z. Hu, X. Nie and G. Cai, Inflammation accelerates copper-mediated cytotoxicity through induction of six-transmembrane epithelial antigens of prostate 4 expression, *Immunol. Cell Biol.*, 2021, **99**, 392–402.

37 M. K. Lesiów, U. K. Komarnicka, K. Stokowa-Sołtys, K. Rolka, A. Łęgowska, N. Ptaszyńska, R. Wieczorek, A. Kyzioł and M. Jeżowska-Bojczuk, Relationship between copper(II) complexes with FomA adhesin fragments of F. nucleatum and colorectal cancer. Coordination pattern and ability to promote ROS production, *Dalton Trans.*, 2018, **47**, 5445–5458.

38 M. K. Lesiów, M. Witwicki, N. K. Tan, M. E. Graziotto and E. J. New, Unravelling the Mystery of COVID-19 Pathogenesis: Spike Protein and Cu Can Synergize to Trigger ROS Production, *Chemistry*, 2023, **29**, e202301530.

39 E. Prenesti, P. G. Daniele, M. Prencipe and G. Ostacoli, Spectrum-structure correlation for visible absorption spectra of copper(II) complexes in aqueous solution, *Polyhedron*, 1999, **18**, 3233–3241.

40 A. Marciniak, M. Cebrat and J. Brasuń, The Coordination Abilities of New Cyclic Analogs of Somatostatin, *Int. J. Pept. Res. Ther.*, 2017, **23**, 135–143.

41 M. K. Lesiów, P. Pietrzyk, A. Bieńko and T. Kowalik-Jankowska, Stability of Cu(II) complexes with FomA protein fragments containing two His residues in the peptide chain, *Metallomics*, 2019, **11**, 1518–1531. Erratum: M. K. Lesiów, P. Pietrzyk, A. Bieńko and T. Kowalik-Jankowska, Stability of Cu(II) complexes with FomA protein fragments containing two His residues in the peptide chain, *Metallomics*, 2020, **12**, 2199.

42 J. Brasuń, A. Matera-Witkiewicz, S. Ołdziej, A. Pratesi, M. Ginanneschi and L. Messori, Impact of ring size on the copper(II) coordination abilities of cyclic tetrapeptides, *J. Inorg. Biochem.*, 2009, **103**, 813–817.

43 K. Panagiotou, M. Panagopoulou, T. Karavelas, V. Dokorou, A. Hagarman, J. Soffer, R. Schweitzer-Stenner, G. Malandrinos and N. Hadjiliadis, Cu(II) and Ni(II) interactions with the terminally blocked hexapeptide Ac-Leu-Ala-His-Tyr-Asn-Lys-amide model of histone H2B (80–85), *Bioinorg. Chem. Appl.*, 2008, **2008**, 257038.

44 D. L. Mendola, A. Magrì, O. Hansson, R. P. Bonomo and E. Rizzarelli, Copper(II) complexes with peptide fragments encompassing the sequence 122–130 of human doppel protein, *J. Inorg. Biochem.*, 2009, **103**, 758–765.

45 E. Székely, M. Molnár, N. Lihi and K. Várnagy, Characterization of Copper(II) and Zinc(II) Complexes of Peptides Mimicking the CuZnSOD Enzyme, *Molecules*, 2024, **29**, 795.

46 M. Medvidović-Kosanović, A. Stanković, M. Drulak and M. Sak-Bosnar, Potentiometric, electrochemical and UV/VIS investigation of a copper(II) complex with β-alanyl-L-histidine, *Int. J. Electrochem. Sci.*, 2018, **13**, 5323–5332.

47 E. V. Suprun, S. A. Khmeleva, S. P. Radko, S. A. Kozin, A. I. Archakov and V. V. Shumyantseva, Direct electrochemical oxidation of amyloid-β peptides via tyrosine, histidine, and methionine residues, *Electrochem. Commun.*, 2016, **65**, 53–56.

48 M. Z. Wiloch, I. Ufnalska, A. Bonna, W. Bal, W. Wróblewski and U. E. Wawrzyniak, Copper(II) Complexes with ATCUN Peptide Analogues: Studies on Redox Activity in Different Solutions, *J. Electrochem. Soc.*, 2017, **164**, G77–G81.

49 M. Lefèvre, L. Lantigner, L. Andolfo, C. Vanucci-Bacque, E. Benoist, C. Esmieu, F. Bedos-Belval and C. Hureau, Reduced Schiffbase derivatives to stop reactive oxygen species production by the Cu(Aβ) species: a structure––activity relationship, *C. R. Chim.*, 2023, **26**, 67–77.

50 S. Rajoriya, S. Bargole and V. K. Saharan, Degradation of a cationic dye (Rhodamine 6G) using hydrodynamic cavitation coupled with other oxidative agents: Reaction mechanism and pathway, *Ultrason. Sonochem.*, 2017, **34**, 183–194.

51 H. J. Brömme, L. Zühlke, R. E. Silber and A. Simm, DCFH2 interactions with hydroxyl radicals and other oxidants–influence of organic solvents, *Exp. Gerontol.*, 2008, **43**, 638–644.

52 N. Bodnár, K. Várnagy, L. Nagy, G. Csire and C. Kállay, Ambivalent role of ascorbic acid in the metal-catalyzed oxidation of oligopeptides, *J. Inorg. Biochem.*, 2021, **222**, 111510.

53 C. Schöneich, Mechanisms of metal-catalyzed oxidation of histidine to 2-oxo-histidine in peptides and proteins, *J. Pharm. Biomed. Anal.*, 2000, **21**, 1093–1097.

54 E. R. Stadtman, Metal ion-catalyzed oxidation of proteins: biochemical mechanism and biological consequences, *Free Radicals Biol. Med.*, 1990, **9**, 315–325.
55 X. Fan, J. Zhang, M. Theves, C. Strauch, I. Nemet, X. Liu, J. Qian, F. J. Giblin and V. M. Monnier, Mechanism of Lysine Oxidation in Human Lens Crystallins during Aging and in Diabetes, *J. Biol. Chem.*, 2009, **284**, 34618–34627.
56 M. Estaras, F. Z. Ameur, M. Estévez, S. Díaz-Velasco and A. Gonzalez, The lysine derivative aminoadipic acid, a biomarker of protein oxidation and diabetes-risk, induces production of reactive oxygen species and impairs trypsin secretion in mouse pancreatic acinar cells, *Food Chem. Toxicol.*, 2020, **145**, 111594.
57 S. Desine, C. L. Gabriel, H. M. Smith, O. R. Antonetti, C. Wang, M. W. Calcutt, A. C. Doran, H. J. Silver, S. Nair, J. G. Terry, J. J. Carr, M. F. Linton, J. D. Brown, J. R. Koethe and J. F. Ferguson, Association of alpha-aminoadipic acid with cardiometabolic risk factors in healthy and high-risk individuals, *Front. Endocrinol.*, 2023, **14**, 1122391.
58 J. C. da Silva, A. U. Amaral, C. Cecatto, A. Wajner, K. D. S. Godoy, R. T. Ribeiro, A. de Mello Gonçalves, Â. Zanatta, M. S. da Rosa, S. O. Loureiro, C. R. Vargas, G. Leipnitz, D. O. G. de Souza and M. Wajner, α-Ketoadipic Acid and α-Aminoadipic Acid Cause Disturbance of Glutamatergic Neurotransmission and Induction of Oxidative Stress In Vitro in Brain of Adolescent Rats, *Neurotoxic. Res.*, 2017, **32**, 276–290.
59 W. Shi, Z. Yang, P. Fu and Y. Yang, Metabolite 2-aminoadipic acid: implications for metabolic disorders and therapeutic opportunities, *Front. Pharmacol.*, 2025, **16**, 1569020.
60 H. M. Irving, M. G. Miles and L. D. Pettit, A study of some problems in determining the stoicheiometric proton dissociation constants of complexes by potentiometric titrations using a glass electrode, *Anal. Chim. Acta*, 1967, **38**, 475–488.
61 P. Gans, A. Sabatini and A. Vacca, SUPERQUAD: an improved general program for computation of formation constants from potentiometric data, *J. Chem. Soc., Dalton Trans.*, 1985, 1195–1200.
62 P. Gans, A. Sabatini and A. Vacca, Investigation of equilibria in solution. Determination of equilibrium constants with the HYPERQUAD suite of programs, *Talanta*, 1996, **43**, 1739–1753.
63 G. Gran, H. Dahlenborg, S. Laurell and M. Rottenberg, Determination of the equivalent point in potentiometric titrations, *Acta Chem. Scand.*, 1950, **4**, 559–577.
64 L. Zékány and I. Nagypál, in *Computational Methods for the Determination of Stability Constants*, ed. D. L. Leggett, Plenum Press, New York, 1985, pp. 291–299.

